The radial age distribution of Galactic Cepheids

Author: Marc Vilanova Sar
Facultat de Física, Universitat de Barcelona, Diagonal 645, 08028 Barcelona, Spain.

Advisor: Friedrich Anders
(Dated: June 16, 2022)

Abstract: The aim of this work is to model the radial age distribution of Galactic Classical Cepheids. We create a simulation of star particles in the Galactic disc using a simple recipe and associate them with stellar evolutionary models. We then select Classical Cepheids from the simulation and test in qualitative terms which definition of the instability strip limits agrees better with the observational data. We show that the two key ingredients for a correct modelling of the observed Galactocentric radius vs. age distribution in the Milky Way are the radial-metallicity gradient and a metallicity dependence of the instability strip.

I. INTRODUCTION

Cepheids are pulsating variable stars that serve as Galactic and extragalactic distance indicators. They are evolved intermediate-to-high mass stars ($3M_\odot - 20M_\odot$) that can be found in the Hertzsprung-Russell diagram (HRD) in the instability strip (IS) region, where they arrive after the main sequence.
The IS is the region in the HRD where pulsating variable stars such as RR Lyrae, W Virginis, δ Scuti, or Cepheids are found (Gautschy & Saio 1996), and its location is conditional on the type of pulsator. The hotter and cooler limits of this region are called the IS's blue and red edges, respectively. The IS occupied by Cepheids is placed hotter than the red-giant branch and extends from hot low-luminosity stars ($T_{\text{eff}} \lesssim 10\,000$ K, $L \gtrsim 2.5L_\odot$) to cold, high-luminosity stars ($T_{\text{eff}} \gtrsim 3\,000$ K, $L \lesssim 5L_\odot$), meaning that more luminous Cepheids tend to be cooler. Despite notable advances in the last decades, the correct modelling of the IS is still an active field, partly due to the lack of accurate observational data for different metallicity and rotation regimes.
There exist mainly two types of Cepheids depending on how they pulsate and their metallicity. Classical Cepheids (CC) are population I stars with regular periods up to 10 days, high metallicity and spectral types from F6 to K2. On the other hand, Type II Cepheids are population II stars with longer periods that vary from 10 to 100 days and low metallicity, meaning they are older. Other types like Anomalous or Double-Mode Cepheids can be found, but they are less abundant.
In this work we will focus only on CCs for the following reasons. They are young (from 20 to 200Myr) and their abundance and luminosity let us trace a significant fraction of the full population. Furthermore, they have a tight period-age relation (see Efremov 1978), which enables us to know their age with precision. This relation can be explained knowing from scratch that Cepheids follow a characteristic pulsating period-luminosity relation (Leavitt 1908), which serves as a distance indicator at Galactic and extragalactic range and relates higher periods to more luminous stars. It was discovered at the beginning of the 20th century and since then it has been one of the most accurate methods to determine distances at the mentioned range. We have to consider two more premises in order to explain the period-age relation, which are the mass-luminosity relation and the stellar age given by the evolutionary models. The first one relates more massive stars to higher luminosities, while stellar evolutionary models associate higher masses with a decrease in the age (Bono et al. 2005). Thus, at longer pulsating periods, we will find younger stars.
Cepheids have a high-density core but a low-density envelope, allowing them to change their radius as much as 20% due to expansion and compression mechanisms during their pulsation stage, when they are not in hydrostatic equilibrium. This phenomenon is the reason why variable stars change their luminosity periodically and it can change up to two magnitudes.
More specifically, when a CC contracts under its gravity, it becomes more opaque and photons get trapped inside. As a consequence of the compression, the pressure inside increases beyond hydrostatic equilibrium, meaning the pressure becomes greater than gravity, causing the star to increase its radius. At this point, the star becomes transparent and radiation can escape, increasing its luminosity. Finally, the star loses the radiative heat given by the photons and begins to cool and compress under its gravity, starting again the cycle. Thus, the star behaves as an harmonic oscillator, always trying to regain the equilibrium point but shooting it past.

CCs have several applications due to their pulsating period-luminosity relation, which is a distance indicator more precise at long distances ($d \gtrsim 500pc$) than the parallax method. They have been used in astronomy to map with high precision not only our Galaxy but also local group galaxies such as the Magellanic Clouds. Some other properties like the Galactic rotational curve, the mass distribution and the dark matter content have been derived thanks to these pulsators (e.g. Ablimit et al. 2020). Likewise, they have allowed the determination of metallicity gradients (e.g. Genovali et al. 2014) and the Galactocentric radius-age distribution.

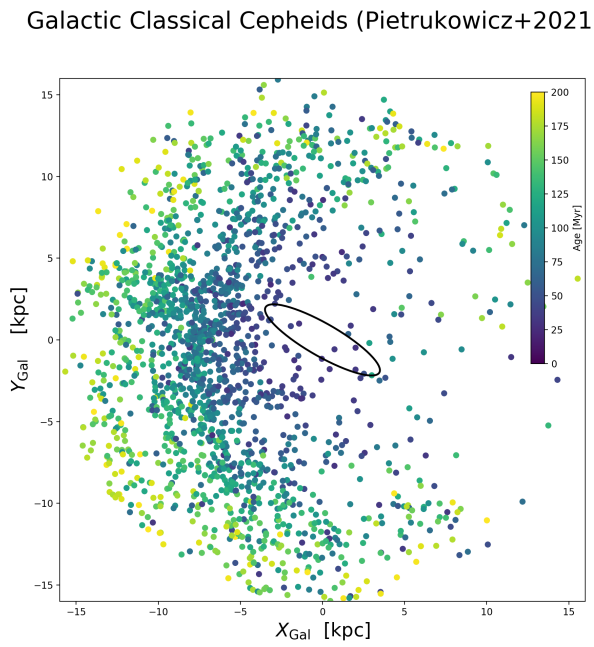

FIG. 1: Distribution of CCs in Galactocentric Cartesian coordinates, colour-coded by age.

A. Galactocentric radius-age relation

Various studies have shown a radial age distribution of Galactic Cepheids (De Somma et al. 2020; Dékány et al. 2019; Pietrukowicz et al. 2021; Skowron et al. 2019). These stars follow a clear negative trend which implies younger stars can be found towards the center of the Galaxy (see Fig. 1). Nevertheless, galaxies are thought to follow an inside-out formation process (Frankel et al. 2019) in order to reproduce the observed size-luminosity-velocity relations, meaning star formation areas expand from the inner parts towards the outer parts of the galaxy as it gets older. Therefore, the observed distribution is counter-intuitive and has to be explained in another way. This misunderstanding can be solved assuming that an inside-out formation process means that although star formation regions expand towards the edges of the galaxy, the star formation rate (SFR) is constant in the inner parts, yielding to the observed distribution.
Moreover, the Besançon Galaxy Model (Mor et al. 2018), which is one of the most efficient models used nowadays to test the Galactic structure, also presents this tendency.

II. OBSERVATIONAL DATA

In this study we are trying to reproduce the data found in Pietrukowicz et al. (2021), which is the largest and most up-to-date catalogue of Galactic CCs available to date. The catalogue gathers observational data from sources like the Optical Gravitational Lensing Experiment (OGLE), ASAS, ASAS-SN, ATLAS, Gaia, NSVS, VVV, WISE, and ZTF (see references in Pietrukowicz et al. 2021). The list only contains 3352 Cepheids in the optical range and all the stars are Gaia EDR3 identified. From the catalogue, we have selected fundamental-mode pulsating CCs, resulting in 2130 stars. For these, we calculated ages following the recipe of Anderson et al. (2016), assuming the Galactic radial abundance gradient of Genovali et al. (2014) and we have selected stars younger than 200Mys. We can see in Fig. 1 how the stars from the catalogue are distributed across the XY Galactic plane, colour-coded by their age, following the distribution explained in section I A.

III. SIMULATIONS

We create a simulation that attempts to model the radial age distribution of Galactic CCs (see Fig. 1), testing different assumptions.
The simulation consists of 3 steps. Firstly, we simulate star particles applying several initial properties. Then we associate each simulated star with stellar evolutionary models. Finally, we define the IS limits and select and study the Cepheids that result from the different modelling assumptions, comparing them to the observational data.

A. Simulated star particles

We create a sample of 10^7 disc star particles using the following initial conditions: an exponentially decreasing density profile, an SFR constant in time (over the past 500 Myr), a constant initial mass function in the range of $3M_\odot - 15M_\odot$ ($\alpha = 2.35$), and an approximate lifetime-mass relation, derived from the PARSEC 1.2S stellar models (Bressan et al. 2012). In order to study how the stars behave in terms of metallicity, we apply the metallicity gradient measured by Genovali et al. (2014). This work has derived one of the most accurate measurements of the Galactic radial abundance gradient based on the observations of 450 Cepheids iron abundances in the Galactocentric distance range of 5-19 kpc.
For this reason, a radial cut has been applied between 4 and 18 kpc. Moreover, for the purpose of filtering which particles corresponded to CC, an age cut has been set since these stars are in an evolved stage of their life, considering only ages greater than 90% of their lifetime. Both filters have given a total number of 248199 possible Cepheids out of the starting sample.

B. Stellar models

Each one of the stars has been associated with stellar evolutionary models. An attempt was made to associate the PARSEC models with the Cepheids

sample, following the trend of the Besançon Galaxy Model, however, there was no clear radial age trend shown, hence, no conclusion could be drawn. Thus, the stars were associated with the BaSTI updated library of stellar evolutionary predictions presented in Hidalgo et al. (2018), which have seemed to agree better with the simulated sample.

BaSTI library provides predictions for two models. On one hand, a convective core overshooting is considered. In this work, however, the stellar model used is given by the Schwarzchild criterion, where the gas is stable against convection. Therefore, no overshooting nor diffusion are considered.

The metrics used in order to associate the star with the closest evolutionary track has been the following:

$$\begin{aligned} d^2 = \quad & (\log \text{age}_{\text{sim}} - \log \text{age}_{\text{BaSTI}})^2 \\ & + (M_{\text{sim}} - M_{\text{BaSTI}})^2 \\ & + ([Fe/H]_{\text{sim}} - [Fe/H]_{\text{BaSTI}})^2 \end{aligned} \tag{1}$$

C. Instability strip

The next step is to determine which of the possible simulated stars are found in the IS, and therefore can be defined as Cepheids, starting by defining its limits.
Some studies have modelled the red and blue edges as constant lines in the HRD (Bono et al. 2000, Fiorentino et al. 2013), not regarding the possible dependence on certain stellar properties, while others have considered a metallicity dependence, since observational data shows that with higher metallicity the IS gets redder (see De Somma et al. (2021)).
This phenomenon can be explained by two reasons: on one hand, as metallicity increases, hydrogen is less abundant, which delays the beginning of pulsation to lower effective temperatures; on the other hand, the increased contribution of iron delays the pulsation to the red edge due to convection. This dependence has been studied and quantified in recent years (e.g. Anderson et al. 2016; De Somma et al. 2021). To test it here, we model the IS limits in two ways, with a dependence on metallicity and without it. In the first case, we consider the recent work of De Somma et al. (2021) where the IS limits are determined for three bins in metallicity: Small Magellanic Cloud (Z=0.004, Y=0.25; their Table 2), Large Magellanic Cloud (Z=0.008, Y=0.25; their Table 3), and M31 (Z=0.03, Y=0.28; their Table 4). By using these 3 definitions, a linear regression has been performed, providing a relation between the blue and red edges with the metallicity of each star. Since the limits defined by De Somma et al. (2021) depend on the absolute metallicity and we want to express our results in terms of the iron-to-hydrogen abundance ratio [Fe/H], we use the canonic transformation [Fe/H]$= 10^{Z-Z_{\odot}}$.
In the second case, we use the definition given by Mor et al. (2017), which has applied the red edge described by Bono et al. (2000) and the blue edge by Fiorentino et al. (2013).

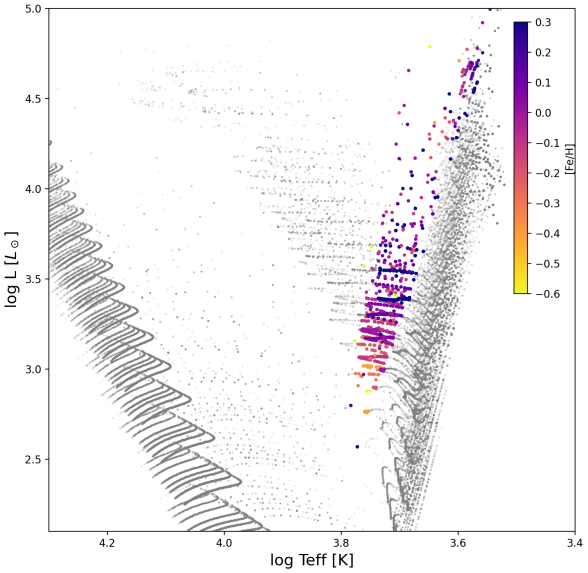

FIG. 2: Simulated population of young stars, using the BaSTI evolutionary models (Hidalgo et al. 2018). The Cepheids, selected from the interpolated IS definition of De Somma et al. (2021), are colour-coded by [Fe/H].

IV. ANALYSIS

First of all, in Fig. 2 we plot the HRD of the simulated stars classified as possible CCs, highlighting the stars inside the IS, colour-coded by metallicity. A total of 248199 stars are distributed in the plot. The IS limits have been defined by the metallicity interpolation explained in section III C and the Genovali et al. (2014) gradient is applied. The region contains 2165 stars.
The objective of this plot is to check out how Cepheids are distributed across the IS depending on their abundance. Nevertheless, this plot shows not only CCs during their pulsation state but also the evolution of stars that due to their initial properties can begin to pulsate at an advanced chapter of their life.
As expected, the IS is found outside the main sequence and close to the giant branch. CCs inside have effective temperatures that vary from 3000K to 6000K and luminosities from 2.5 $L_{\odot}$ up to 5$L_{\odot}$.
Bearing in mind the metallicity dependence on the IS limits, we should see an increase in metallicity towards the red edge. The aforementioned distribution is barely seen, with a slight tendency of metal-rich stars at lower temperatures in the IS and an accumulation of metal-

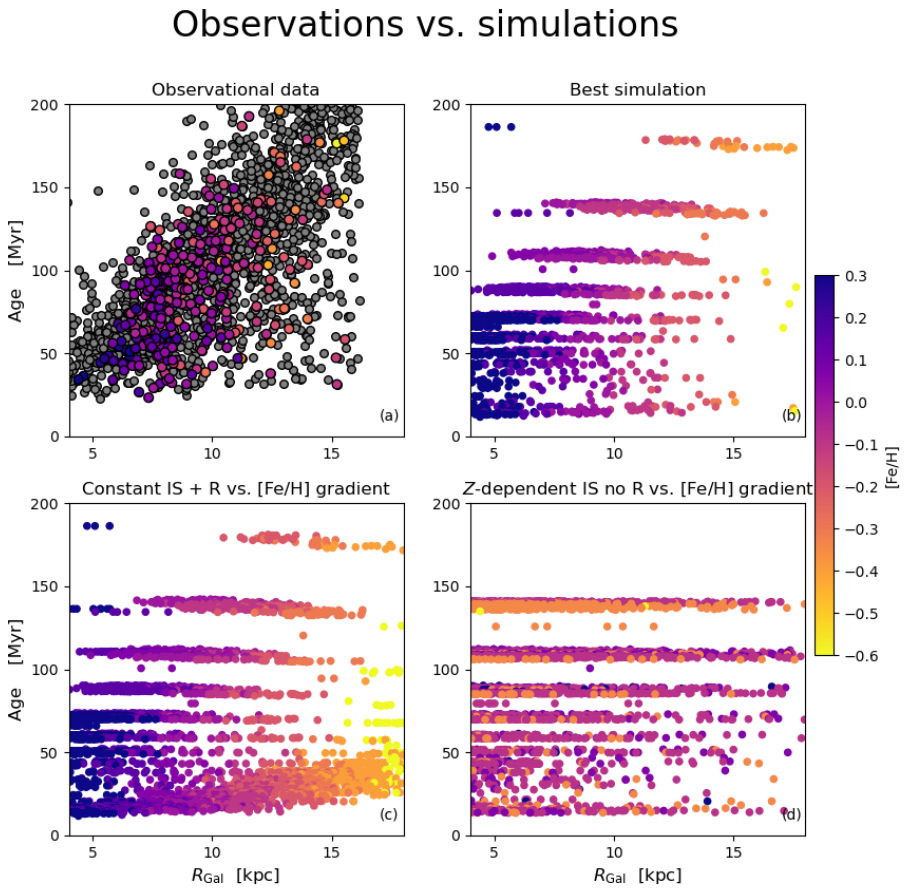

FIG. 3: Age vs Galactocentric radius for observed and simulated CCs colour-coded by metallicity. Top left: Observational data from Pietrukowicz et al. (2021), colour-coded (when available) by spectroscopic metallicities from Genovali et al. (2014) and Kovtyukh et al. (2022). Top right: Simulated Cepheids with metallicity-dependent IS and Galactic [Fe/H] gradient applied. Bottom left: Simulated Cepheids with constant IS and [Fe/H] gradient applied. Bottom right: Simulated Cepheids with metallicity-dependent IS and no [Fe/H] gradient applied.

poor stars at low luminosities, which is not representative enough.

A. Radial age distribution

The next step is to study the simulated Cepheids inside the different IS limits by comparing their radial age distribution to the observational data presented in Pietrukowicz et al. (2021) (see Fig. 3(a)). Due to the lack of spectroscopic data, only 378 out of the 1892 observed stars have a measured [Fe/H], given by Genovali et al. (2014) and Kovtyukh et al. (2022).
In Fig. 3(b) and (c) the Genovali et al. (2014) metallicity gradient is applied, whereas in Fig. 3(d) it has not been used, which creates a difference between the plots not only in the metallicity distribution but also in the age distribution. These differences are going to be described and compared to the observational data.

In Fig. 3(b), where the metallicity dependence is applied, the radial-age distribution follows a negative age trend towards the center, which agrees fairly with the observational data seen in Fig. 3(a). The IS modelled here contains 2165 Cepheids.

Considering the constant IS definition, the radial-age distribution is presented in Fig. 3(c). In this case, 3739 stars are found inside the IS. We can see that this profile is less clear than the one with the IS metallicity dependence, and there is an accumulation of young stars at Galactocentric distances higher than 15 kpc. This can be explained by assuming that the IS limits are wider than the ones considering metallicity dependence, and simulated stars that may not be classified as CCs are found in the IS.

In Fig. 3(d), the metallicity dependence is applied. However, there is no clear trend observed since there is no metallicity gradient, which confirms that stars in our

Galaxy follow an abundance profile similar to the one determined by Genovali et al. (2014). This modelled IS contains 3139 stars.

Comparing the 3 simulated distributions, we can conclude that the one that agrees better with the observational data from Pietrukowicz et al. (2021) is Fig. 3(b); hence, the best model of the IS has to consider a metallicity dependence on its limits, confirming that with higher metallicities the IS limits get redder, therefore, colder. We can also affirm that the Genovali et al. (2014) gradient is another key ingredient in the simulation, since the model is better when metal-rich stars are close to the inner parts of the Galaxy and metal-poor stars are found towards the outer parts.
Finally, we can see some age discontinuities of the stars in all the simulations made. This is caused by the metrics used (see eq. (1)) in order to associate the stars with the closest stellar evolutionary model found in BasTI.

V. CONCLUSIONS

We have created a simulation with a sample of star particles that has tried to model the radial age distribution of Galactic CCs. These particles were created applying a series of simple assumptions, including a constant initial mass function, an exponential decreasing disc profile, a constant SFR, and a relation between the star mass and its lifetime. Moreover, we have applied the metallicity gradient found in Genovali et al. (2014) and have compared it with a simulation without this gradient. The simulated stars have been associated with evolutionary tracks from the BaSTI group.
To select CCs, we have modelled the IS limits considering a metallicity dependence, interpolating the values found in De Somma et al. (2021), in order to define a blue and red edge for all the possible abundances in the sample, which covered a range from the Small Magellanic Cloud metallicity (Z=0.004) to M31 metallicity (Z=0.03). Another definition of the IS has been considered, with no metallicity dependence (Mor et al. (2017)) and the Genovali et al. (2014) gradient. For the sake of comparing these different IS modellings, we have filtered the CCs for each of these simulations and have studied their Galactocentric radial-age distribution.
Even though the two definitions considering the Genovali et al. (2014) gradient have seemed to follow the observational data (see Fig. 3 (a)), the one that has shown to be the best model is the metallicity interpolation, showing a clear trend where younger stars were found in the inner parts of the Galaxy, whereas older stars were found towards the outer disc, in agreement with the data from Pietrukowicz et al. (2021). On the other hand, the definition without including the Genovali et al. (2014) gradient has not shown the observational trend at all, demonstrating that the inclusion of the radial metallicity gradient is a key ingredient in the simulation.

In light of the statements expressed above, we can conclude that the IS has to have a metallicity dependence on its limits in order to model the observational data in Pietrukowicz et al. (2021), following the trend of works like De Somma et al. (2020); Dékány et al. (2019); Skowron et al. (2019). Moreover, our results also indicate that the Galactic radial metallicity gradient is a key ingredient in the simulation of Galactic Classical Cepheids.

Acknowledgments

I would like to thank my advisor, Friedrich Anders, for his time and valuable counsel, it has been a pleasure working with him. Many thanks also to my family and friends for their patience and support.

Ablimit, I., Zhao, G., Flynn, C., & Bird, S. A. 2020, ApJ, 895, L12
Anderson, R. I., Saio, H., Ekström, S., Georgy, C., & Meynet, G. 2016, A&A, 591, A8
Bono, G., Caputo, F., Cassisi, S., et al. 2000, ApJ, 543, 955
Bono, G., Marconi, M., Cassisi, S., et al. 2005, ApJ, 621, 966
Bressan, A., Marigo, P., Girardi, L., et al. 2012, MNRAS, 427, 127
De Somma, G., Marconi, M., Cassisi, S., et al. 2020, MNRAS, 496, 5039
De Somma, G., Marconi, M., Cassisi, S., et al. 2021, MNRAS, 508, 1473
Dékány, I., Hajdu, G., Grebel, E. K., & Catelan, M. 2019, ApJ, 883, 58
Efremov, I. N. 1978, Soviet Ast., 22, 161
Fiorentino, G., Musella, I., & Marconi, M. 2013, MNRAS, 434, 2866
Frankel, N., Sanders, J., Rix, H.-W., Ting, Y.-S., & Ness, M. 2019, ApJ, 884, 99
Gautschy, A. & Saio, H. 1996, ARA&A, 34, 551
Genovali, K., Lemasle, B., Bono, G., et al. 2014, VizieR Online Data Catalog, J/A+A/566/A37
Hidalgo, S. L., Pietrinferni, A., Cassisi, S., et al. 2018, ApJ, 856, 125
Kovtyukh, V., Lemasle, B., Bono, G., et al. 2022, MNRAS, 510, 1894
Leavitt, H. S. 1908, Annals of Harvard College Observatory, 60, 87
Mor, R., Robin, A. C., Figueras, F., & Antoja, T. 2018, A&A, 620, A79
Mor, R., Robin, A. C., Figueras, F., & Lemasle, B. 2017, A&A, 599, A17
Pietrukowicz, P., Soszyński, I., & Udalski, A. 2021, Acta Astron., 71, 205
Skowron, D. M., Skowron, J., Mróz, P., et al. 2019, Science, 365, 478